Production of negative hydrogen ions within MMS Fast Plasma Investigation due to solar wind bombardment

Imogen Gingell[1], Steven J. Schwartz[1,2], Daniel J. Gershman[3], William R. Paterson[3], Ravindra T. Desai[1], Barbara L. Giles[3], Craig J. Pollock[3], Levon A. Avanov[3]

[1]The Blackett Laboratory, Imperial College London, SW7 2AZ, United Kingdom
[2]Laboratory for Atmospheric and Space Physics, University of Colorado, Boulder, Colorado 80303, USA
[3]NASA, Goddard Space Flight Center, Greenbelt, Maryland 20771, USA

Key Points:

- An anomalous population is observed by MMS's electron plasma instruments in the solar wind.
- The population is consistent with negative ions generated by charge exchange within the instrument.
- The errors in the calculation of the electron moments are estimated.

Corresponding author: Imogen Gingell, i.gingell@imperial.ac.uk

Abstract

The particle data delivered by Fast Plasma Investigation (FPI) instrument aboard NASA's Magnetospheric Multiscale (MMS) mission allows for exceptionally high-resolution examination of the electron and ion phase space in the near-Earth plasma environment. It is necessary to identify populations which originate from instrumental effects. Using FPI's Dual Electron Spectrometers (DES) we isolate a high energy (∼keV) beam, present while the spacecraft are in the solar wind, which exhibits an azimuthal drift with period associated with the spacecraft spin. We show that this population is consistent with negative hydrogen ions H^- generated by a double charge exchange interaction between the incident solar wind H^+ ions and the metallic surfaces within the instrument. This interaction is likely to occur at the deflector plates close to the instrument aperture. The H^- density is shown to be approximately 0.2-0.4% of the solar wind ion density, and the energy of the negative ion population is shown to be 70% of the incident solar wind energy. These negative ions may introduce errors in electron velocity moments on the order of 0.2-0.4% of the solar wind velocity, and significantly higher errors in the electron temperature.

1 Introduction

The Magnetospheric Multiscale (MMS) mission [*Burch et al.*, 2016a] is a multi-spacecraft magnetospheric plasma physics platform launched in 2015. It provides exceptional time and angular resolution for both field and particle data, with up to two orders of magnitude greater cadence than its most recent predecessors Cluster and THEMIS. Understanding the limitations of in situ plasma instruments is critical to the analysis of the data they provide to MMS and future space missions, and informs the design and operation of the next generation of instruments.

The Fast Plasma Investigation [*Pollock et al.*, 2016] (FPI) aboard MMS comprises the Dual Electron Spectrometers (DES) to measure the electron phase space density, and the Dual Ion Spectrometers (DIS) to measure the ion phase space density. Each spacecraft includes 4 DES and DIS units, each of which includes two top-hat electrostatic analysers. The eight total sensor heads each for DES and DIS are distributed around the spacecraft spin plane such that the spacecraft samples the full 4π solid angle sky at any given time. The instrument cadence for the full sky phase space is 0.03s for DES and 0.15s for DIS. The "skymaps" supplied by both DES and DIS instruments are composed of 16 polar angle bins, 32 azimuthal angle bins, and 32 energy bins in the range 2eV to 30keV for the events discussed in this paper. These instruments measure the energy per unit charge E/q, and thus do not distinguish particles by mass or charge state.

Given the high spatial and temporal resolution together with instrument calibration required to meet the MMS mission objectives, it is important to separate signals generated by the ambient plasma environment from those generated by instrumentation effects. This is especially important in regions for which kinetic plasma processes are significant, and associated non-gyrotropic particle populations are common. The MMS mission targets several of these regions, such as the bow shock [*Johlander et al.*, 2016] or the diffusion regions of magnetic reconnection sites [*Burch et al.*, 2016b]. In these regions, characterisation of the full ion or electron phase space is critical to understanding of microphysics processes.

In this paper, we identify an apparently non-gyrotropic population observed by FPI-DES while the MMS spacecraft are in the solar wind. We examine the properties of this anomalous population, and show that it is consistent with negative hydrogen ions H^- generated by interaction of the solar wind with metallic surfaces internal to the DES instrument.

2 Observations

An example of an anomalous periodic signal visible within the DES "electron" distribution function is shown in Figure 1. Here, we present a period for which the MMS spacecraft are upstream of the quasi-perpendicular bow shock, and two minutes of burst mode data have been collected while the spacecraft are within the solar wind. The burst data of interest are shown for 2017 January 5th, 05:02:10 UTC to 05:04:05 UTC.

For this event, a population is visible with approximately anti-sunward flow velocity ($130° < \phi < 230°$) in the energy range $831eV < E < 1423eV$. The population exhibits a drift in observed flow azimuth from 130° to 230° over a period of $2.5s$. The time-averaged skymaps shown in Figure 2 for this energy range indicate that this population is narrowly distributed in polar flow angle θ, with angular distribution similar to the solar wind in the same energy range. Additionally, these skymaps demonstrate that the anomalous population is not organised by the local magnetic field. This population is present within the distribution functions derived from FPI-DES for all four MMS spacecraft.

We note that in this energy range, the count rates recorded by the DES instrument are very low. Typically, the population appears in ∼10 solid angle bins within the skymap for a given energy. In each given time interval $\delta t = 0.03s$, each bin records 1-3 counts. As such, time-averaged and angle-integrated distribution functions help to recognise the trend. There are other known sources of background electrons, including both spacecraft photoelectrons and internal secondary electrons [*Gershman et al.*, 2017]. These affect primarily the low energy ($\approx$ 10eV) measurements. We have verified that the phase space densities associated with these electrons are approximately two orders of magnitude smaller than those shown in Figure 2. Removing these known background populations from the distribution function data does not significantly affect the anomalous population of interest, as shown in Figure 3. Similarly, we have also verified that this periodic population is not an artefact of compression of the data [*Barrie et al.*, 2017], which is lossless for this period.

The azimuthal flow dependence of the anomalous population observed by the DES displays a period of 2.5s. The spin period of the MMS spacecraft is approximately 20 seconds and each spacecraft has 8 DES sensor heads aboard. Hence, a 2.5s interval corresponds to the period over which each DES sensor head is sampling the plasma from within 45° of a given azimuthal look direction, e.g. the Earth-Sun line. Since the population appears in all four spacecraft, this suggests that while the population is instrumental, the generation of that population is driven by a common, external environmental factor. In this case, we will show that that driver is likely to be the solar wind proton flux. Timing offsets of the anomalous population between the spacecraft are thus attributed to differences in spacecraft spin phase, rather than motion of an ambient population.

3 Negative Ions

It is well established that bombardment of metallic surfaces by positively charged ions can generate negatively charged ions by double charge-exchange interactions [*Maazouz et al.*, 1996], $H^+ + 2e^- \rightarrow H^-$. The FPI-DES instruments measure only the energy per unit charge E/q for negatively charged particles, and cannot distinguish particles by species. It is therefore possible that the instrument registers negative ions in addition to the expected high energy electron population. Indeed, similar electron spectrometer instruments have been utilised to observe ambient negative ion populations in other environments, including at comets [*Chaizy et al.*, 1991; *Burch et al.*, 2015] and in the Saturnian system [*Coates et al.*, 2007, 2010; *Teolis et al.*, 2010], where determination of the bulk properties of the population can be non-trivial [*Desai et al.*, 2017].

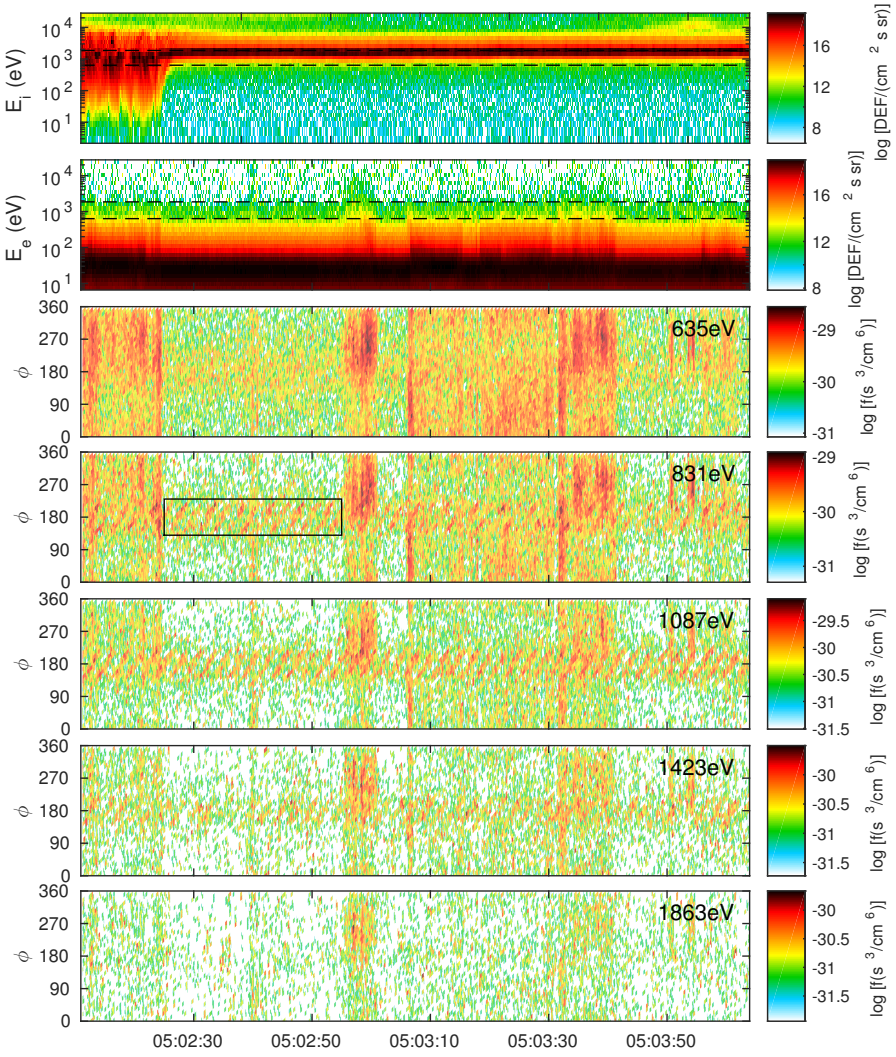

Figure 1. Top panel: Differential energy flux (colour) for FPI-DIS, with the energy range of the lower panels shown with dashed lines. Second panel: Differential energy flux for FPI-DES. Lower panels: Flow azimuth dependence of the phase space density (colour) for FPI-DES, integrated over the polar angle, for several energy bins over which the population exhibiting azimuthal drift is observable. Data are shown for 2017 January 5th, 05:02:10 UTC to 05:04:05 UTC. The anomalous population is visible throughout, but is the only population clearly visible for the interval 05:02:25 to 05:02:55 UTC, for example. During this time interval, the anomalous population is shown with a black box in the 831eV energy bin; the energy bin for which its phase space density is highest.

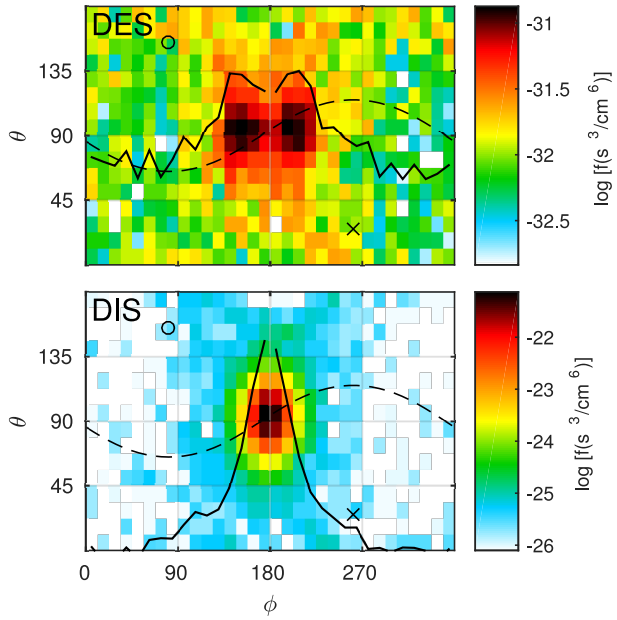

Figure 2. Phase space density (colour) as a function of azimuthal and polar flow angle, for the DES (top) and DIS (bottom) instruments, averaged over the time interval 05:02:31 to 05:02:55 UTC (shown in Figure 1 as a black box) and over the energy range $831eV < E < 1423eV$. The centre of the plots, for which $\theta = 90°$ and $\phi = 180°$, correspond to the anti-sunward flow direction. The direction parallel to the mean magnetic field for this interval is shown with an 'o', anti-parallel with an 'x', and the 90° pitch angle contour is shown as a black dashed line. The phase space density averaged over the polar angle is shown as a black line, and its vertical axis coincides with the colour bar.

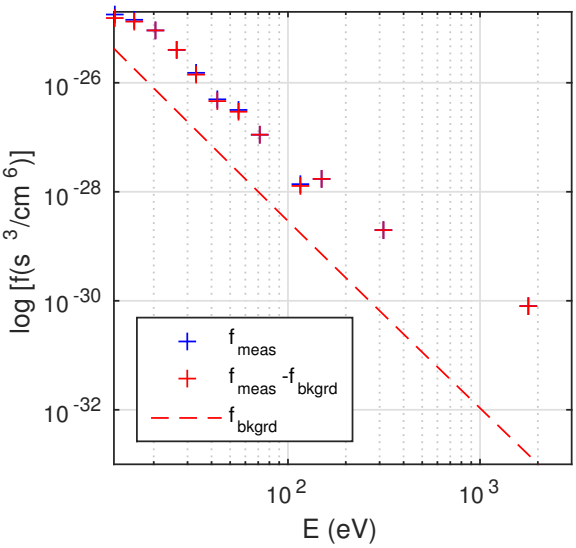

Figure 3. Phase space density as a function of energy for a single angular element of a skymap which includes the anomalous population at $\sim$ $2keV$. The total phase space density measured by DES $f_{\mathrm{meas}}(E)$ and the background electron population $f_{\mathrm{bkgrd}}(E)$ are shown. For energy bins associated with the anomalous population, the measured phase space density is two orders of magnitude greater than the background.

If the anomalous population observed by the DES is negative H^- ions generated by charge exchange interactions of the solar wind H^+ beam with metallic surfaces within the instrument, we can expect the anomalous DES population to exhibit the following properties:

1. For specular reflection of solar wind ions from a metallic surface within the DES instrument, the registered azimuthal flow angle of the H^- will drift as the orientation of the DES instrument changes relative to the incident flow. With only one DES sensor head in optimal alignment at any given time, we would expect the period of the azimuthal drift to be 2.5s, as we have already demonstrated in Figure 1.
2. The H^- population will be strongly localised in flow direction, similar to the incident solar wind ion beam. In contrast to typical solar wind electron populations, it will therefore appear non-gyrotropic and will not be organised by the local magnetic field. These properties have been demonstrated in Figure 2.
3. The H^- population should always be present where we observe significant positive ion flux, as in the solar wind. However, clear signatures such as azimuthal drift of the H^- beam may only be present if the solar wind beam is narrow.
4. The conversion rate for $\sim$keV H^+ to H^- has been shown [*Maazouz et al.*, 1996] to be up to 5% for 1keV H^+. Conversion is weakly dependent on angle of incidence for oblique collisions, with rate reducing to $\sim$ 0.1% for grazing collisions due to surface roughness effects. Given this dependence, and given that the DES instrumentation may not record all negative ions generated by these double charge exchange interactions, we expect an upper-bound on the density of observed H^- on the order of or less than 0.1-5% of the solar wind ion density.
5. For an elastic collision, the energy of negative ions generated by double charge exchange with metallic surfaces is expected to be strongly correlated with the so-

Table 1. Events and associated solar wind and H^- parameters. Mean solar wind ion energy $< E_{sw,i} >$ is derived from FPI-DIS. Average negative ion energy $< E_{H^-} >$ is determined the energy bin of FPI-DES which displays the highest density of H^-.

Date/time (UTC)	H^- seen?	$< E_{sw,i} > (eV)$	$< E_{H^-} > (eV)$
2015 10 07 061144	Y	899	750
2015 10 21 101044	N	266	-
2015 11 03 081104	Y	959	1089
2015 11 04 045734	Y	2723	1791
2015 11 04 050654	Y	2123	1582
2015 11 04 052804	Y	2628	1791
2015 11 04 061134	Y	2570	1791
2015 11 04 080514	Y	2443	1582
2015 12 28 061654	Y	1040	750
2016 01 11 053744	Y	811	663
2016 12 09 111804	Y	1705	1087
2016 12 21 120804	N	1953	-
2016 12 22 105614	Y	1270	1087
2016 12 23 071914	Y	2574	1863
2017 01 05 050133	Y	1405	831

lar wind H^+ energy. Deviations should be correlated with the angle of emergence from the surface, reflecting the inelastic aspects of the collision of the H^+ ion with the instrument surface.

In order to test these properties, we have examined the DES-derived distribution function in the ∼keV range for 15 events captured in burst mode for which the MMS spacecraft are in the solar wind. The parameters of the solar wind and apparent H^- populations for each of these events are summarised in Table 1. Of the events examined, all but two exhibited a ∼keV population with characteristic azimuthal drift. For these null events, the solar wind ion temperature reported by FPI-DIS is high, and the H^- population may not be visible because it has been spread too thinly across several energy bins in the DES-derived distribution function. Together, this survey suggests that the anomalous DES population is near ubiquitous in the solar wind. This supports the hypothesis that this population comprises instrument-induced H^-.

We can examine the flux of H^- using the count rates within FPI-DES for the full phase space. Assuming that the phase space density $f(\mathbf{v})$ varies slowly over a given region of the d^3v velocity space, $f(\mathbf{v})$ is related to the counts C measured by FPI according to the following equation [*Pollock et al.*, 2016]:

$$\frac{C}{\tau} = (\hat{\mathbf{n}} \cdot \mathbf{v}) f(\mathbf{v}) G \mathrm{d}^3 v, \tag{1}$$

where G is the geometric factor, τ is the accumulation time, $\hat{\mathbf{n}}$ is the normal to the instrument aperture, and $\hat{\mathbf{n}} \cdot \mathbf{v} \approx v$ when accounting only for particles which enter the instrument aperture. The number density n for a given species is determined by taking moments of the phase space density:

$$n = \int f(\mathbf{v}) \mathrm{d}^3 v, \tag{2}$$

or equivalently $\mathrm{d}n = f(\mathbf{v})\mathrm{d}^3v$ for a single element of phase space. The number density within a given energy-angle bin $\mathrm{d}n$ is therefore related to the counts as follows:

$$\mathrm{d}n = \frac{C}{G\tau}\frac{1}{v} = \frac{C}{G\tau}\sqrt{\frac{m}{2(E/q)|Ze|}}. \tag{3}$$

Equation 3 relates the number density of particles, assumed to have mass m and charge Ze, to the count rate C in a given energy channel (E/q) of the electrostatic detector.

Taking the sum over many energy-angle bins, each with count C_i and energy channel $(E/q)_i$, the density of electrons is therefore:

$$n_e = \sqrt{\frac{m_e}{2e}}\frac{1}{G_e\tau}\sum_i \frac{C_i}{\sqrt{(E/q)_i}}. \tag{4}$$

Likewise, the density of H^- is given by:

$$n_{H^-} = \sqrt{\frac{m_p}{2e}}\frac{1}{G_{H^-}\tau}\sum_i^{H^-} \frac{C_i}{\sqrt{(E/q)_i}}, \tag{5}$$

Here, the sum $\sum_i^{H^-}$ is performed only over regions of phase space dominated by H^-.

Hence, the number density of H^- compared to the electron density n_{H^-}/n_e is derived from the counts as follows:

$$\frac{n_{H^-}}{n_e} \approx \sqrt{\frac{m_p}{m_e}}\frac{G_e}{G_{H^-}}\frac{\sum_i^{H^-} C_i/\sqrt{(E/q)_i}}{\sum_j C_j/\sqrt{(E/q)_j}}. \tag{6}$$

The geometric factors G incorporate a response function for FPI-DES to electrons and negative ions, respectively. In the absence of data for the response of FPI-DES to negative ions, we assume for simplicity that the response for negative hydrogen at ∼1keV is similar to the response to protons and electrons as reported by *Peko and Stephen* [2000]; *Ladislas Wiza* [1979]. In that case, the ratio G_e/G_{H^-} is assumed to be approximately unity. For a quasi-neutral plasma $n_e \approx n_i \approx n_{H^+}$; the relative density of negative ions to incoming solar wind protons is therefore given by

$$\frac{n_{H^-}}{n_{H^+}} \approx \sqrt{\frac{m_p}{m_e}}\frac{\sum_i^{H^-} C_i/\sqrt{(E/q)_i}}{\sum_j^{e} C_j/\sqrt{(E/q)_j}}. \tag{7}$$

This relative density n_{H^-}/n_{H^+} is shown alongside the sum over the counts $\sum_i C_i/\sqrt{E_i}$ for both electrons and H^- for the 2017 January 5th 05:01:33 UTC event in Figure 4. The negative ion counts C_{H^-} are integrated over the region of phase space for which H^- signatures are visible for this event: $135° < \phi < 235°$, $45° < \theta < 135°$ and $484eV < E < 2440eV$. This demonstrates that the density of H^- is on the order of 0.2-0.4% of the incoming solar wind density. This is towards the lower range of conversion rates of keV H^+ to H^- by double charge exchange reported by *Maazouz et al.* [1996]. Given our assumption of approxmately equal micro channel plate (MCP) efficiencies for negative hydrogen and electrons in the ∼keV range (i.e. $G_e/G_{H^-} \approx 1$), this represents a lower bound for the conversion rate.

Finally, to further verify surface charge exchange as a likely mechanism for production of H^-, we determine the energies of both the incident solar wind beam and the apparent negative ion population. The mean solar wind energy is determined for each event

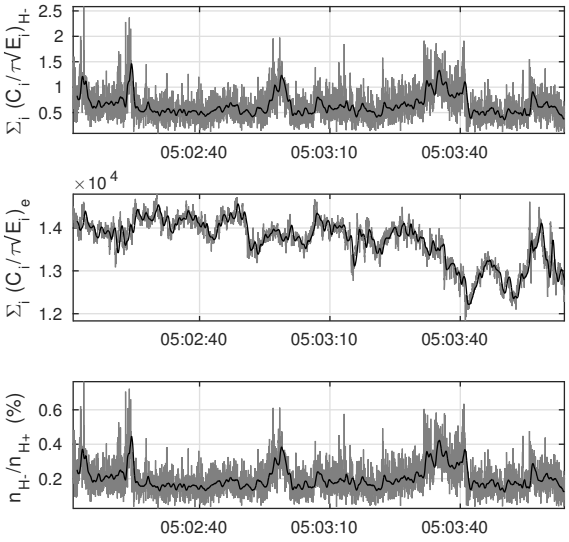

Figure 4. Top: Time dependence of the total counts from DES within the region of phase space dominated by H^-. Middle: Time dependence of the total counts for the full phase space from DES, approximating the electron density. Bottom: Ratio of the H^- to electron number densities, derived from the upper panels according to Equation 7. The instantaneous counts are shown in grey, and the 1s moving average is shown in black.

from the mean of the bulk speed while MMS1 is within the undisturbed solar wind. Given the difficulty with separation of the H^- population from thermal electrons in the lower solar wind energy cases, the approximate average H^- energy is taken to be the centre of the DES energy bin for which the H^- population is most dense. These average energies are given in Table 1.

The relationship between solar wind ion and negative ion energies is shown in Figure 5. The error bars associated with the negative ion energy are chosen such that the limits are centres of the maximum and minimum DES energy bins at which the negative ion population are clearly observed. Figure 5 demonstrates that the energy of the negative ion population is linearly proportional to the incident solar wind energy, such that $E_{H^-} \approx 0.7E_{H^+}$. This trend is consistent with the production of H^- with the solar wind as a driver, and suggests that approximately 30% of the energy in the solar wind ions is lost during inelastic collision with the spacecraft surfaces. Although this relationship isn't necessarily unique to the proposed mechanism of production, it provides further evidence in favour of this interpretation in combination with the previous analysis.

4 Effect on Electron Moments

Given the existence of a negative ion population with number density $n_{H^-} \approx 0.2\% n_e$, we can estimate the effect on derived electron moments, where data processing has assumed that all particles reported by FPI-DES are electrons. Considering that the counts are due to real electrons together with H^- ions treated as though they were also electrons, we can split the calculated "electron" phase space distribution into its two sources,

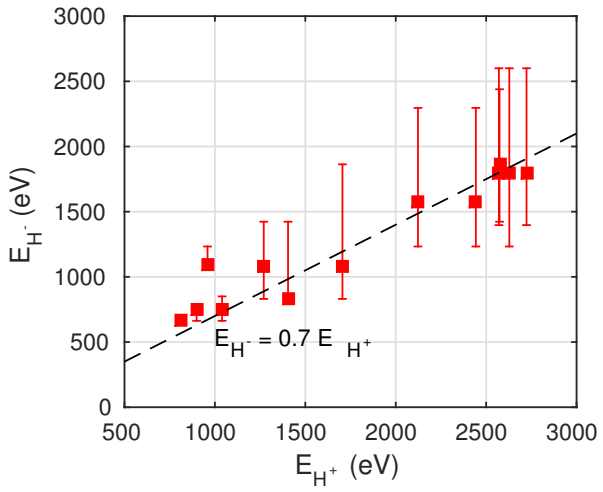

Figure 5. Dependence of the energy of the negative ion H^- population as a function of the energy of the incident solar wind proton beam, for the events listed in Table 1. Error bars represent the maximum and minimum energies at which the H^- population is visible within the distribution function data. A dashed line represents the line of best fit, with equation $E_{H^-} = 0.7 E_{H^+}$.

e.g.

$$f(\mathbf{v}) = f_e(\mathbf{v}) + f_{H-}(\mathbf{v}) \tag{8}$$

We integrate this to find the inferred electron density n_e^*

$$\begin{aligned} n_e^* &= \int f(\mathbf{v})\, d^3v & (9)\\ &= \int f_e(\mathbf{v})\, d^3v + \int f_{H-}(\mathbf{v})\, d^3v & (10)\\ &\approx n_e + dn' & (11) \end{aligned}$$

where dn' is the electron density inferred from counts in the energy bins contaminated by H^- ions. From Equation 3 we can write dn' as

$$\begin{aligned} dn' &= \frac{C_{H-}}{G_e \tau}\sqrt{\frac{m_e}{2e(E/q)_{H-}}} & (12)\\ &= \frac{C_{H-}}{G_{H-}\tau}\sqrt{\frac{m_p}{2e(E/q)_{H-}}}\frac{G_{H-}}{G_e}\sqrt{\frac{m_e}{m_p}}, & (13) \end{aligned}$$

where $(E/q)_{H^-}$ denotes the energy channel dominated by H^- ions. Given the actual density of negative ions n_{H-} derived in Equation 5,

$$dn' = n_{H-}\frac{G_{H-}}{G_e}\sqrt{\frac{m_e}{m_p}}. \tag{14}$$

Hence for $n_{H-}/n \approx 0.2\%$ and $G_{H-}/G_e \approx 1$, we find that the error in the electron number density is $dn'/n \approx 0.005\%$. Thus we see that mistaking the H^- ions as electrons has a negligible impact on the calculation of the electron density.

Higher order moments can be treated the same way, e.g.

$$\begin{aligned} n < v_x > &= n_e < v_x >_e + f_{H-}\, d^3v\, v_x & (15)\\ &\approx n_e < v_x >_e - n_{H-}\frac{G_{H-}}{G_e}\sqrt{\frac{m_e}{m_p}}\, V_{e,(E/q)_{H-}} & (16) \end{aligned}$$

where $V_{e,(E/q)_{H-}}$ is the electron velocity (taken here to be in the $-x$ direction) associated with the (E/q) bin contaminated by H^- ions, and we have used (14) to re-write $f_{H-}\, d^3v \equiv dn'$. We can estimate $V_{e,(E/q)_{H-}}$ as

$$V_{e,(E/q)_{H-}} \equiv \sqrt{\frac{2e(E/q)_{H^-}}{m_e}} \tag{17}$$

$$= \sqrt{\frac{m_p}{m_e}}\, V_{H^-} \sim \sqrt{\frac{m_p}{m_e}}\, V_{\rm sw}, \tag{18}$$

where the velocity of the H^- population V_{H^-} is approximately the solar wind velocity $V_{\rm sw}$. Thus the particle flux moment, assuming $G_{H-} = G_e$ for simplicity, becomes

$$n < v_x > = n_e(-V_{\rm sw}) - n_{H-}V_{\rm sw} \tag{19}$$

$$= -(n_e + n_{H-})\, V_{\rm sw}. \tag{20}$$

The bulk velocity is therefore given by:

$$< v_x > \approx -V_{\rm sw} - \frac{n_{H-}}{n} V_{\rm sw}. \tag{21}$$

The estimated error in the reported bulk velocity is given by the second term in Equation 21: $\delta V/V_{SW} \approx n_{H-}/n$. We note that n_{H-} refers to the true number density of H^- generated by charge exchange, rather than its effect on the reported electron number density dn', given in Equation 14. Hence the reported bulk velocity moment includes an estimated 0.2% error due to the influence of the H^-. For typical solar wind velocity $V_{\rm sw} = 750{\rm kms}^{-1}$, this error is $\delta V \approx 2{\rm kms}^{-1}$. These errors are not significant except in spectral analysis of the velocity moments, where low-amplitude spectral components may be important to consider.

Successive higher moments will introduce additional factors of $\sqrt{m_p/m_e}$ to the contaminating component, neglecting the vectorial aspects of the velocity $\mathbf{v}$. The contribution to the stress tensor, while still small, will be proportionally larger than the impact on the density and bulk flow velocity.

When calculating the electron moments, any significant errors in higher order moments such as the electron temperature may be reduced by integrating only over regions of the reported DES phase space that do not contain H^- signals, rather than using the full distribution function. However, this method requires that the H^- population is well separated from the ambient electron population.

5 Discussion

Using a set of analyses detailed in Section 3, we have shown that the anomalous ∼keV negatively-charged population visible in the DES-derived distribution function is consistent with negative hydrogen ions. These negative ions are produced by double charge exchange interactions of incident solar wind protons with the metallic surfaces within the DES sensor heads. Given their location close to the instrument aperture, the deflector plates are likely responsible. For a diagram showing the location of the deflector plates see *Pollock et al.* [2016], Figure 7. These deflector plates allow for control of azimuth look direction [*Pollock et al.*, 2016], and similar design principles are used in near-future missions such as Parker Solar Probe [*Kasper et al.*, 2016] and Solar Orbiter. A population of H^- may also be generated by collisions of solar wind ions with the double grid across the instrument aperature, however given the 90% transmission rate of the grid [*Pollock et al.*, 2016] the effect is likely to be relatively minor. Furthermore, we note that the $\sim 90^\circ$ range of the azimuthal drift of the H^- population in Figure 1 and the double-peaked distribution of H^- in Figure 2 suggest that conditions are met for the detection of H^- in up to two DES sensor heads at a given time.

We have shown in Figure 4 that the production of negative ions may introduce errors in the reported electron bulk velocity moments of less than one percent. Although this error may be acceptable where bulk properties are concerned, and in many cases is below the typical noise, it may introduce significant uncertainty when considering the spectral properties of the electron moments in the solar wind. Given that the study of turbulence in the solar wind is an objective of the near-future in situ space missions such as Solar Orbiter and Parker Solar Probe, it is necessary to determine whether H^- is being produced by the interaction of the solar wind with their instrumentation. Although production of H^- by double charge exchange may also occur within the magnetosheath and magnetopause, H^- is not expected to affect the analysis and conclusions of studies of electron-scale reconnection, such as *Burch et al.* [2016b]. For these cases, any signatures of H^- would be well separated from important agyrotropic electron populations in phase space.

Observable signatures of instrument-induced production of H^- are highly dependent on spacecraft and instrument configuration. H^- may be identified in particle data as a highly non-gyrotropic population, with correlation of apparent flow angle with the flow angle of the incident solar wind (as in Figure 2), and correlation of the mean energy of the H^- with the solar wind ion energy (as in Figure 5).

The azimuthal drift of the H^- population demonstrated in Figure 1 will only be visible if the spacecraft, and therefore the instrument, rotates with respect to the incident solar wind velocity. For example, the PEACE instrument aboard Cluster [*Johnstone et al.*, 1997] and the ESA instrument aboard THEMIS [*McFadden et al.*, 2008] will not observe azimuthal drift of any instrument-induced H^- simply because the time resolution of the data is equal to the spin period of the spacecraft. Similarly, the future mission Solar Orbiter will not observe azimuthal drift because the particle instruments will not rotate with respect to the solar wind bulk flow, excepting minor fluctuations of the bulk velocity within the solar wind. Lack of azimuthal drift will not affect the apparent density of H^- for these spacecraft. Instead, H^- will appear spread across a consistent set of azimuthal bins during each spin period. This may make H^- more difficult to identify.

Further, the spacecraft materials exposed to the solar wind, particularly within the instrument itself, will affect the both the production and observation of the population. For these reasons, the form of H^- signals presented in this paper are unlikely to be exactly reproduced in other spacecraft.

6 Conclusions

This study demonstrates that instrument-induced negative ions are a contributor to the apparent electron phase space densities in the solar wind proton energy range. In view of ongoing MMS operations and near-future in situ space physics missions, it is important to test for the presence of these negative ions, and to remove their influence on derived electron moments where possible. With respect to the long-term future of in situ space missions, it may be useful to test for the generation of H^- by double charge exchange before launch.

Acknowledgments

This work was supported by the UK Science and Technology Facilities Council (STFC) grant ST/N000692/1. Data used in this research is publically available at the MMS Science Data Center at the Laboratory for Atmospheric and Space Physics (LASP) hosted by the University of Colorado, Boulder (https://lasp.colorado.edu/mms/sdc/public/).

References

Barrie, A. C., S. E. Smith, J. C. Dorelli, D. J. Gershman, P. Yeh, C. Schiff, and L. A. Avanov (2017), Performance of a space-based wavelet compressor for plasma count data on the MMS Fast Plasma Investigation, *Journal of Geophysical Research (Space Physics)*, *122*, 765–779, doi:10.1002/2016JA022645.

Burch, J. L., T. E. Cravens, K. Llera, R. Goldstein, P. Mokashi, C.-Y. Tzou, and T. Broiles (2015), Charge exchange in cometary coma: Discovery of H^- ions in the solar wind close to comet 67P/Churyumov-Gerasimenko, *Geophys. Res. Lett.*, *42*, 5125–5131, doi:10.1002/2015GL064504.

Burch, J. L., T. E. Moore, R. B. Torbert, and B. L. Giles (2016a), Magnetospheric Multiscale Overview and Science Objectives, *Space Sci. Rev.*, *199*, 5–21, doi:10.1007/s11214-015-0164-9.

Burch, J. L., R. B. Torbert, T. D. Phan, L.-J. Chen, T. E. Moore, R. E. Ergun, J. P. Eastwood, D. J. Gershman, P. A. Cassak, M. R. Argall, S. Wang, M. Hesse, C. J. Pollock, B. L. Giles, R. Nakamura, B. H. Mauk, S. A. Fuselier, C. T. Russell, R. J. Strangeway, J. F. Drake, M. A. Shay, Y. V. Khotyaintsev, P.-A. Lindqvist, G. Marklund, F. D. Wilder, D. T. Young, K. Torkar, J. Goldstein, J. C. Dorelli, L. A. Avanov, M. Oka, D. N. Baker, A. N. Jaynes, K. A. Goodrich, I. J. Cohen, D. L. Turner, J. F. Fennell, J. B. Blake, J. Clemmons, M. Goldman, D. Newman, S. M. Petrinec, K. J. Trattner, B. Lavraud, P. H. Reiff, W. Baumjohann, W. Magnes, M. Steller, W. Lewis, Y. Saito, V. Coffey, and M. Chandler (2016b), Electron-scale measurements of magnetic reconnection in space, *Science*, *352*, aaf2939, doi:10.1126/science.aaf2939.

Chaizy, P., H. Reme, J. A. Sauvaud, C. D'Uston, R. P. Lin, D. E. Larson, D. L. Mitchell, K. A. Anderson, C. W. Carlson, A. Korth, and D. A. Mendis (1991), Negative ions in the coma of Comet Halley, *Nature*, *349*, 393–396, doi:10.1038/349393a0.

Coates, A. J., F. J. Crary, G. R. Lewis, D. T. Young, J. H. Waite, and E. C. Sittler (2007), Discovery of heavy negative ions in Titan's ionosphere, *Geophys. Res. Lett.*, *34*, L22103, doi:10.1029/2007GL030978.

Coates, A. J., G. H. Jones, G. R. Lewis, A. Wellbrock, D. T. Young, F. J. Crary, R. E Johnson, T. A. Cassidy and T. W. Hill (2010), Negative ions in the Enceladus plume, *Icarus*, *206*, 618–622, doi:10.1016/j.icarus.2009.07.013.

Desai, R. T., A. J. Coates, A. Wellbrock, V. Vuitton, F. J. Crary, D. González-Caniulef, O. Shebanits, G. H. Jones, G. R. Lewis, J. H. Waite, M. Cordiner, S. A. Taylor, D. O. Kataria, J.-E. Wahlund, N. J. T. Edberg, and E. C. Sittler (2017), Carbon Chain Anions and the Growth of Complex Organic Molecules in Titan's Ionosphere, *Astrophys. J. Lett.*, *844*, L18, doi:10.3847/2041-8213/aa7851.

Gershman, D. J., L. A. Avanov, S. A. Boardsen, J. C. Dorelli, U. Gliese, A. C. Barrie, C. Schiff, W. R. Paterson, R. B. Torbert, B. L. Giles, and C. J. Pollock (2017), Spacecraft and instrument photoelectrons measured by the dual electron spectrometers on mms, *Journal of Geophysical Research: Space Physics*, pp. n/a–n/a, doi:10.1002/2017JA024518, 2017JA024518.

Johlander, A., S. J. Schwartz, A. Vaivads, Y. V. Khotyaintsev, I. Gingell, I. B. Peng, S. Markidis, P.-A. Lindqvist, R. E. Ergun, G. T. Marklund, F. Plaschke, W. Magnes, R. J. Strangeway, C. T. Russell, H. Wei, R. B. Torbert, W. R. Paterson, D. J. Gershman, J. C. Dorelli, L. A. Avanov, B. Lavraud, Y. Saito, B. L. Giles, C. J. Pollock, and J. L. Burch (2016), Rippled Quasiperpendicular Shock Observed by the Magnetospheric Multiscale Spacecraft, *Physical Review Letters*, *117*(16), 165101, doi:10.1103/PhysRevLett.117.165101.

Johnstone, A. D., C. Alsop, S. Burge, P. J. Carter, A. J. Coates, A. J. Coker, A. N. Fazakerley, M. Grande, R. A. Gowen, C. Gurgiolo, B. K. Hancock, B. Narheim, A. Preece, P. H. Sheather, J. D. Winningham, and R. D. Woodliffe (1997), Peace: a Plasma Electron and Current Experiment, *Space Sci. Rev.*, *79*, 351–398, doi:

10.1023/A:1004938001388.

Kasper, J. C., R. Abiad, G. Austin, M. Balat-Pichelin, S. D. Bale, J. W. Belcher, P. Berg, H. Bergner, M. Berthomier, J. Bookbinder, E. Brodu, D. Caldwell, A. W. Case, B. D. G. Chandran, P. Cheimets, J. W. Cirtain, S. R. Cranmer, D. W. Curtis, P. Daigneau, G. Dalton, B. Dasgupta, D. DeTomaso, M. Diaz-Aguado, B. Djordjevic, B. Donaskowski, M. Effinger, V. Florinski, N. Fox, M. Freeman, D. Gallagher, S. P. Gary, T. Gauron, R. Gates, M. Goldstein, L. Golub, D. A. Gordon, R. Gurnee, G. Guth, J. Halekas, K. Hatch, J. Heerikuisen, G. Ho, Q. Hu, G. Johnson, S. P. Jordan, K. E. Korreck, D. Larson, A. J. Lazarus, G. Li, R. Livi, M. Ludlam, M. Maksimovic, J. P. McFadden, W. Marchant, B. A. Maruca, D. J. McComas, L. Messina, T. Mercer, S. Park, A. M. Peddie, N. Pogorelov, M. J. Reinhart, J. D. Richardson, M. Robinson, I. Rosen, R. M. Skoug, A. Slagle, J. T. Steinberg, M. L. Stevens, A. Szabo, E. R. Taylor, C. Tiu, P. Turin, M. Velli, G. Webb, P. Whittlesey, K. Wright, S. T. Wu, and G. Zank (2016), Solar Wind Electrons Alphas and Protons (SWEAP) Investigation: Design of the Solar Wind and Coronal Plasma Instrument Suite for Solar Probe Plus, *Space Sci. Rev.*, *204*, 131–186, doi:10.1007/s11214-015-0206-3.

Ladislas Wiza, J. (1979), Microchannel plate detectors, *Nuclear Instruments and Methods*, *162*, 587–601, doi:10.1016/0029-554X(79)90734-1.

Maazouz, M., R. Baragiola, A. Borisov, V. A. Esaulov, S. Lacombe, J. P. Gauyacq, L. Guillemot, and D. Teillet-Billy (1996), H $^-$ formation in the scattering of hydrogen ions on an Al surface, *Surface Science*, *364*, L568–L574, doi:10.1016/0039-6028(96)00771-6.

McFadden, J. P., C. W. Carlson, D. Larson, M. Ludlam, R. Abiad, B. Elliott, P. Turin, M. Marckwordt, and V. Angelopoulos (2008), The THEMIS ESA Plasma Instrument and In-flight Calibration, *Space Sci. Rev.*, *141*, 277–302, doi:10.1007/s11214-008-9440-2.

Peko, B. L., and T. M. Stephen (2000), Absolute detection efficiencies of low energy H, H, H+, H2+ and H3+ incident on a multichannel plate detector, *Nuclear Instruments and Methods in Physics Research Section B: Beam Interactions with Materials and Atoms*, *171*, 597–604, doi:10.1016/S0168-583X(00)00306-2.

Pollock, C., T. Moore, A. Jacques, J. Burch, U. Gliese, Y. Saito, T. Omoto, L. Avanov, A. Barrie, V. Coffey, J. Dorelli, D. Gershman, B. Giles, T. Rosnack, C. Salo, S. Yokota, M. Adrian, C. Aoustin, C. Auletti, S. Aung, V. Bigio, N. Cao, M. Chandler, D. Chornay, K. Christian, G. Clark, G. Collinson, T. Corris, A. De Los Santos, R. Devlin, T. Diaz, T. Dickerson, C. Dickson, A. Diekmann, F. Diggs, C. Duncan, A. Figueroa-Vinas, C. Firman, M. Freeman, N. Galassi, K. Garcia, G. Goodhart, D. Guererro, J. Hageman, J. Hanley, E. Hemminger, M. Holland, M. Hutchins, T. James, W. Jones, S. Kreisler, J. Kujawski, V. Lavu, J. Lobell, E. LeCompte, A. Lukemire, E. MacDonald, A. Mariano, T. Mukai, K. Narayanan, Q. Nguyan, M. Onizuka, W. Paterson, S. Persyn, B. Piepgrass, F. Cheney, A. Rager, T. Raghuram, A. Ramil, L. Reichenthal, H. Rodriguez, J. Rouzaud, A. Rucker, Y. Saito, M. Samara, J.-A. Sauvaud, D. Schuster, M. Shappirio, K. Shelton, D. Sher, D. Smith, K. Smith, S. Smith, D. Steinfeld, R. Szymkiewicz, K. Tanimoto, J. Taylor, C. Tucker, K. Tull, A. Uhl, J. Vloet, P. Walpole, S. Weidner, D. White, G. Winkert, P.-S. Yeh, and M. Zeuch (2016), Fast Plasma Investigation for Magnetospheric Multiscale, *Space Sci. Rev.*, *199*, 331–406, doi:10.1007/s11214-016-0245-4.

Teolis, B. D., G. H. Jones, P. F. Miles, R. L Tokar, B. A Magee, J. H Waite, E. Roussos, D. T. Young, F. J. Crary, A. J. Coates, R. E. Johnson, W.-L. Tseng, and R. A. Baragiola (2010), Cassini Finds an Oxygen-Carbon Dioxide Atmosphere at Saturn's Icy Moon Rhea, *Science*, *330*, 1813, doi:10.1126/science.1198366.